Hindawi
Geofluids
Volume 2021, Article ID 5562532, 14 pages
https://doi.org/10.1155/2021/5562532

Research Article

A Comparative Study of the Micropore Structure between the Transitional and Marine Shales in China

Pengfei Jiao,[1] **Genshun Yao**,[1] **Shangwen Zhou**,[1,2,3] **Zhe Yu**,[1,2,3] **and Shiluo Wang**[1,2,3]

[1]*PetroChina Research Institute of Petroleum Exploration & Development, Beijing 100083, China*
[2]*National Energy Shale Gas R&D (Experiment) Center, Langfang 065007, China*
[3]*Key Lab of Unconventional Oil & Gas, CNPC, Langfang 065007, China*

Correspondence should be addressed to Shangwen Zhou; zhousw10@petrochina.com.cn

Received 24 January 2021; Revised 9 March 2021; Accepted 25 March 2021; Published 8 April 2021

Academic Editor: Zhiye Gao

To compare the micropore structure of marine-continental transitional shale with marine shale, organic geochemical, field emission scanning electron microscopy, and low-temperature nitrogen adsorption experiments were conducted on shale samples from the Shanxi Formation in the eastern Ordos Basin and the Longmaxi Formation in the southern Sichuan Basin. The results show that Shanxi Formation shale has a smaller specific surface area and pore volume than Longmaxi Formation shale; therefore, the transitional shales fail to provide sufficient pore spaces for the effective storage and preservation of natural gas. Both the transitional and marine shales are in an overmature stage with high total organic carbon content, but they differ considerably in pore types and development degrees. Inorganic pores and fractures are dominantly developed in transitional shales, such as intragranular pores and clay mineral interlayer fractures, while organic nanopores are rarely developed. In contrast, organic pores are the dominant pore type in the marine shales and inorganic pores are rarely observed. The fractal analysis also shows that pore structure complexity and heterogeneity are quite different. These differences were related to different organic types, i.e., type I of marine shale and type III of transitional shale. Marine Longmaxi shale has experienced liquid hydrocarbon cracking, gas generation, and pore-forming processes, providing good conditions for natural gas to be preserved. However, during the evolution of transitional Shanxi shale, gas cannot be effectively preserved due to the lack of the above evolution processes, leading to the poor gas-bearing property. The detailed comparison of the micropore structure between the transitional and marine shales is of great importance for the future exploitation of marine-continental transitional shale gas in China.

1. Introduction

After the shale gas successes in North America, China's shale gas exploration and development has achieved great achievements in marine shales, especially in the southern Sichuan Basin [1–4]. In 2020, China reported total shale gas production of 20 billion cubic meters. Marine shale gas in China is mainly developed in the Upper Ordovician Wufeng-Lower Silurian Longmaxi Formation, where the depositional environment is stable and changes progressively from deep-sea shelf facies to shallow-sea shelf facies, featuring large thickness, vast distribution, and good continuity [5, 6]. Previous studies have covered the depositional sediment, reservoir characteristics, and main constraints for the enrichment and high yield of the marine shale in the Sichuan Basin, especially about its pore development and relating mechanisms [7–9]. In the Sichuan Basin, Wufeng-Longmaxi Formation marine shale features high TOC, with the organic maturity generally in the high maturity stage to the overmature stage and the organic type commonly being type I or type II_1, promising good hydrocarbon-generating potential [10–12]. The mineral contents are principally quartz minerals and secondarily clay minerals. Carbonate minerals are relatively developed, and pyrite is developed in many layers. Shale has good brittleness, which is beneficial to hydrofracturing operation [13, 14].

The field emission scanning electron microscope (FE-SEM) images indicate that the marine shale has organic nanopores of various shapes: irregular organic matter pores are mainly developed in the primary organic matter, and the spongy and dense round bubble pores are mainly developed in the solid bitumen [15–17]. The image quantitative analysis method can be used to extract organic pores in FE-SEM images and count their pore size distribution (PSD) and surface porosity (SP), and it is found that mesopores (2 nm-50 nm) and micropores (<2 nm) are mainly developed in marine shale [18–20]. The shape of the low-temperature nitrogen adsorption (LTNA) curve shows that the Longmaxi shale is dominated by ink bottle pores and parallel plate pores [21]. There are many factors affecting the development of organic matter pores in marine shale. It is generally believed that the higher the organic carbon content, the more developed the organic pores [22, 23]. Various minerals also have different effects on the development of organic matter pores [24–27]. As to the genesis of the organic nanopores, it is assumed that they mainly come from gas generation by kerogen pyrolysis [28, 29] and raw oil (bitumen) cracking [30–32].

Compared with marine shale, less attention has been paid to marine-continental transitional shale, which is mostly found in delta facies where rapid microfacies changes have caused the marine-continental transitional shale to be thinner and less continuous, making it more difficult to be developed [33, 34]. However, the transitional shale gas resources are large, about 19.8×10^{12} m^3 [35], and marine-continental transitional shale will be the future research highlight for shale gas exploration and development in China. The establishment of a complete set of the marine-continental transitional shale gas theory will fill the gap of the unconventional oil and gas theory. At present, the organic geochemistry, mineral composition, and micropore structure characteristics of marine-continental transitional shale in the Longtan Formation of the Sichuan Basin and the Shanxi Formation of the Ordos Basin have been studied. The research shows that the transitional shale has high TOC, its organic maturity varies from place to place, and it is usually in the high maturity stage, and the kerogen type is mainly type III or type II_2 [36]. Clay minerals are the main components, most of which are montmorillonite or illite/smectite mixed layers [37–39].

Four types of pores are developed in the transitional facies shale, which are clay mineral pores, organic matter pores, brittle mineral pores, and microfractures. Clay mineral pores are dominant, followed by brittle mineral pores and organic matter pores [40, 41]. The LTNA curve shape of the transitional shale is similar to that of the marine shale, indicating that the mesopores with the ink bottle shape and parallel plate shape are mainly developed [42, 43]. It can be found that the main pore development types of marine shale and marine-continental transitional shale are very different. Some scholars think that it is caused by different types of kerogen [44, 45]. Some researchers believe that the clay mineral content is the main factor affecting the pore development of marine-continental transitional shale [46].

Although some basic studies have been carried out on the marine-continental transitional shale and the micropore structure characteristics have been preliminarily understood, few scholars have compared and analyzed the pore development characteristics of the two types of shale. In particular, the reason for their differences has not been deeply analyzed, which is very important for the future exploration of transitional shales. In the present study, we investigated the micropore structure characteristics of marine-continental transitional shale from the Shanxi Formation in the eastern Ordos Basin by FE-SEM and LTNA tests and FHH fractal analysis. And we also made some comparisons between transitional shales and marine shales, focusing on the pore development of marine-continental transitional shale and its geological significance.

2. Geological Settings

The Ordos Basin, located in the west of the North China plate, is composed of six secondary structural units: Yimeng uplift, Tianhuan depression, Northern Shanxi slope, Western margin thrust belt, Weibei uplift, and West Shanxi flexural belt [47]. The Permian strata in the eastern margin of the Ordos Basin were developed in marine-continental transitional facies deposits, which can be divided into Shanxi, Benxi, and Taiyuan Formations. The Shanxi Formation is dominated by delta facies, while the Benxi and Taiyuan Formations were developed in delta, lagoon, tidal flat, and shallow shelf deposits from north to south. In the vertical directions, mudstone is distributed alternately with coal and sandstone, and pure mudstone is rarely developed. The thickness of mudstone in Benxi, Taiyuan, and Shanxi Formations is about 10–30 m, 20–30 m, and 70–100 m, respectively. Therefore, the mudstone of the Shanxi Formation is preferred as the research object of marine-continental transitional shale in this area. The studied shale samples are from the Daning-Jixian block in the southern end of the West Shanxi flexural belt and the southern margin of the Yishan slope, Ordos Basin (Figure 1). Its tectonic setting is relatively gentle and simple, and the fault is not developed, which is characterized by "one uplift and one depression and two slopes." In the Shan-2 member of the Daning-Jixian block, the mudstone thickness is primarily ranging from 40 m to 70 m.

The Sichuan Basin is located on the western edge of the Upper Yangtze Platform, surrounded by many orogenic belts [48]. The marine Longmaxi Formation in the Sichuan Basin is dominated by shelf facies with stable sedimentary facies belts and wide distribution. The deep-water shelf sediments are developed in the southern and northeastern Sichuan Basin. The studied shale samples from the Longmaxi Formation in the Taiyang-Dazhai block belong to deep-water shelf sediments, located in the low fold structural belt of the southern Sichuan Basin, which presents a structural pattern of "three sags, one uplift," i.e., Luobu-Daba syncline, Yunshanba syncline, Baiyangping syncline, and Taiyang anticline (Figure 2). The shale thickness of the Taiyang-Dazhai block is about 100-170 m, which is larger than that of the Daning-Jixian block.

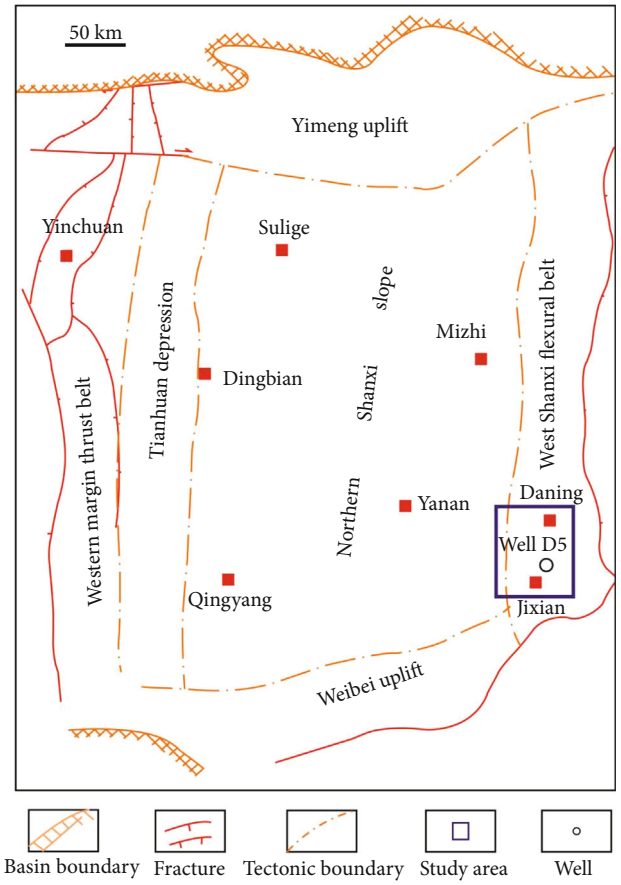

Figure 1: Daning-Jixian block in the eastern Ordos Basin.

3. Samples and Experiments

3.1. Samples. A total of 32 shale samples were collected from the Shanxi Formation of well D5 in the eastern Ordos Basin (16 samples) and from the Longmaxi Formation of well Y5 in the southern Sichuan Basin (16 samples). The locations of the 2 wells are shown in Figures 1 and 2, respectively. Well D5 is located in the Daning-Jixian block, and well Y5 is situated in the Taiyang-Dazhai block. These samples will be tested as follows.

3.2. Field Emission Scanning Electron Microscopy (FE-SEM). The shale samples were imaged with an FEI Helios 650 field emission scanning electron microscope (FE-SEM). Backscattering electron (BSE) mode images well discriminate different minerals and organic matters (voltage 5 kV, current 1.6 nA, and maximum resolution 2 nm), while secondary electron (SE) mode images can well distinguish organic matters and pores (voltage 10 kV, current 0.4 nA, and maximum resolution 2 nm) [49]. The shale samples were cut into approximately 1 cm thick pieces that are parallel between the upper and lower parts. The observation surface was ground with 400-, 800-, 1000-, and 2000-mesh sandpaper to mirror-smooth, then polished again with diamond water, cleaned, and kept in a 105°C incubator for 2 days. The observation surface of the sample was then polished and carbon-plated with a PECS II 685 argon ion polisher to make the observation surface smoother and enhance the electrical conductivity of the sample.

3.3. Low-Temperature Nitrogen Adsorption (LTNA). The surface area and porosity analyzer ASAP 2420 produced by Micromeritics Company was used to conduct LTNA experiments on shale samples crushed to 200-mesh sandpaper at 77 K. The saturated vapor pressure p_0 of N_2 is 0.11117 MPa, and the maximum equilibrium pressure of the experiment is the atmospheric pressure (0.1013 MPa) to deliver a wide N_2 adsorption and desorption isothermal line ($p/p_0 = 0.0095 - 0.995$, where p is the equilibrium pressure). The Barrett-Joyner-Halenda (BJH) method can be used to analyze the mesopore distribution and calculate the average pore size and PV [50]. The SSA of the sample can be derived by the Brunauer-Emmett-Teller (BET) process [51, 52]. The average pore size, total pore volume, and specific surface area of the two shales were compared and analyzed to further characterize their differences.

3.4. Fractal Method. The FHH fractal approach features a simple model expression and operation principle, and it follows the classic theory of multilayer adsorption [53]. The multilayer adsorption on the surface of mesopores in shale can be explained by the following expression:

$$\theta = \frac{V}{V_m} = k \cdot \left(-\ln \frac{p}{p_0}\right)^{-f(D)} = k \cdot \left(\ln \frac{p_0}{p}\right)^{-f(D)}, \quad (1)$$

where θ is the surface coverage of adsorbed molecules; V is the adsorption quantity at the equilibrium pressure, cm^3/g; V_m is the maximum adsorption capacity of the monolayer, cm^3/g; p is the equilibrium pressure, MPa; and p_0 is the saturated vapor pressure of the adsorbate, MPa. k is the characteristic constant, and $f(D)$ is the expression of fractal dimension D of mesopores. Take the logarithm on both sides of Equation (1) to get

$$\ln V = -f(D) \cdot \ln \ln \frac{p_0}{p} + \ln V_m + \ln k. \quad (2)$$

In Equation (2), $\ln V$ is linear to $\ln\ln(p_0/p)$, and $-f(D)$ is the slope of a linear equation. According to Ismail and Pfeifer [54], at the beginning of N_2 adsorption, the number of adsorbed molecular layers is less, and the relation of $f(D)$ with fractal dimension D conforms to the following expression:

$$f(D) = \frac{3 - D}{3}. \quad (3)$$

When there are more molecular layers, capillary condensation will take place. Then, the relation of $f(D)$ with fractal dimension D conforms to the following equation:

$$f(D) = 3 - D. \quad (4)$$

So, the fractal dimension analysis of mesopores was made

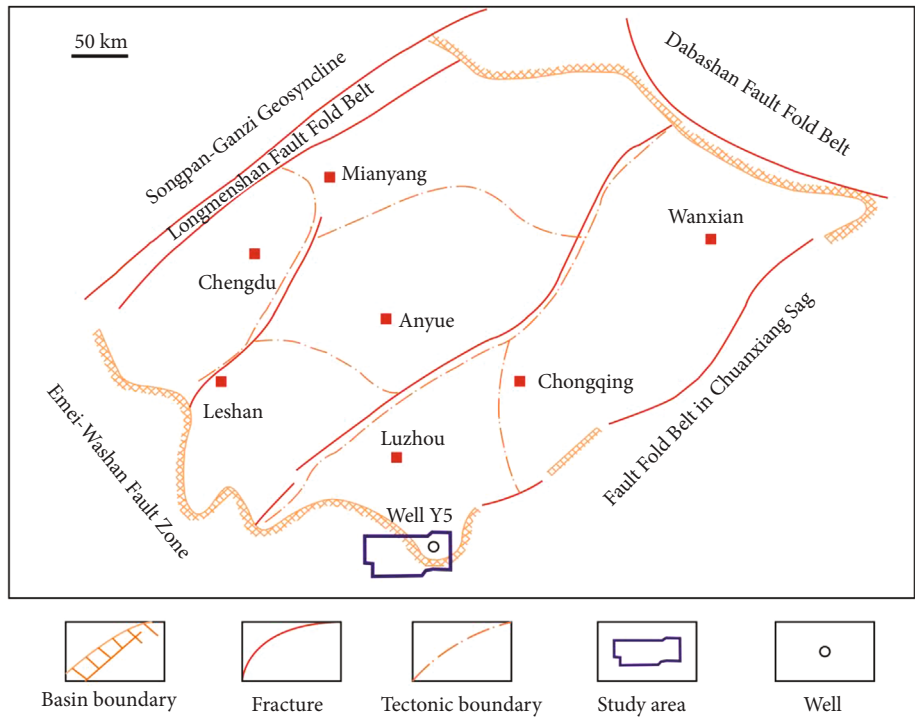

Figure 2: Taiyang-Dazhai block in the south of the Sichuan Basin.

over two stages: initial N_2 adsorption when there are fewer adsorbed molecular layers and later N_2 adsorption when there are more adsorbed molecular layers and capillary condensation takes place.

4. Results

4.1. Organic Geochemistry and Mineral Compositions. The TOC values of the transitional shale are 0.45%–15% with an average of 3.92%. About 60% of the transitional shale samples have TOC content greater than 2%. The organic maturity is 1.92%–2.60% with an average of 2.36%, suggesting a gas-generating peak stage. As the organic type is type III, it mainly produces gas. Among the marine shale samples, the TOC is 1.07%–6.18% with an average of 2.89%. The organic maturity is 2.47%–2.79% with an average of 2.59%, suggesting an overmature gas-generating stage. The organic type is mainly type I and partially type II_1.

Shanxi Formation shale has a relatively high clay mineral content and quartz content, with an average of 47.81% and 40%, respectively, but they fluctuate greatly. Only very few samples contain carbonate minerals (Figure 3(a)). Kaolinite is the main clay mineral, followed by illite and smectite mixed layers; illite content is low; some samples contain a small amount of chlorite. Longmaxi Formation shale has slightly lower clay minerals than quartz minerals, with an average of 29.40% for clay minerals and 34.60% for quartz minerals. Carbonate minerals are very developed with an average of 27.80% (Figure 3(b)). The clay minerals are mostly illite/smectite mixed layers and secondarily illite. Chlorite is well developed, and kaolinite is not found.

4.2. Pore Morphology from FE-SEM. After argon ion polishing and carbon plating on shale samples, their SEM images were obtained by FE-SEM. The SE mode images can clearly distinguish organic matters and organic pores. Organic maters are darker than other minerals and grayish-black in color. The halo generated on the edge of organic pores can well determine the size of the organic pores. In Shanxi Formation shale, the organic matters are typically loose lumps. A small amount of organic matter locally developed dense bubble pores of different sizes (Figure 4(a)). Most of the organic matters contain a few angular organic pores (Figure 4(b)). In addition, some organic matter developed marginal fractures or a small number of angular pores in the part contacting with minerals (Figure 4(c)). The quartz and feldspar minerals mostly contain angular and elliptical intragranular pores (Figure 4(d)). Dissolution pores can be seen in a few calcite and feldspar minerals. Inside the pyrite framboids, angular intercrystalline pores are frequently encountered (Figure 4(e)). Clay minerals represent the main mineral type for Shanxi Formation shale, and they are predominantly smectite and illite/smectite mixed layers; hence, slit clay mineral pores and clay mineral interlayer fractures are very developed (Figure 4(f)). Marine-continental transitional shale mainly features various types of inorganic pores, with slit clay mineral pores and clay mineral interlayer fractures being the most developed, followed by brittle mineral intragranular pores.

Unlike Shanxi Formation shale, there are numerous nanoscale organic pores with pore size mostly ranging from dozens up to hundreds of nanometers inside the organic matters of Longmaxi Formation shale. Most of the organic matters contain large amounts of bubble pores about

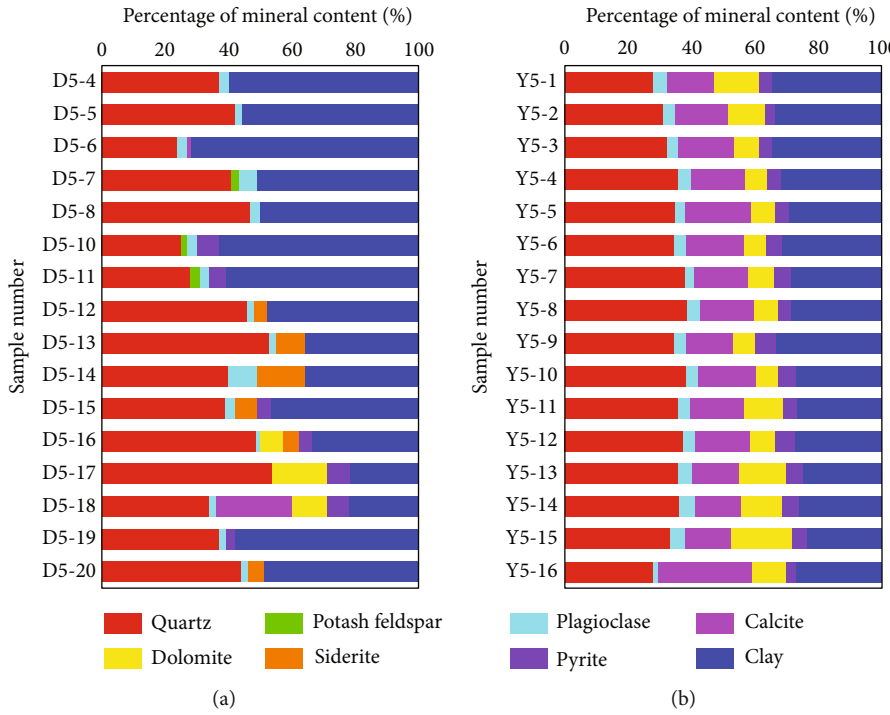

Figure 3: Mineral percentage content bar chart of (a) Shanxi Formation shale and (b) Longmaxi Formation shale.

100 nm in size (Figure 5(a)), and fused macropores composed of a number of bubble pores contacted together are very common. Irregular primary pores are developed in a few organic matters. Pyrite is well developed in marine shale, which is associated with organic matter. Organic pores inside these organic matters are very developed and relatively small in size (Figure 5(c)). As to mineral matrix pores, in addition to angular intragranular pores in brittle minerals like quartz, feldspar, and calcite (Figure 5(d)), slit-shaped or wedge-shaped intergranular pores are often observed on the edge of some brittle minerals (Figure 5(e)). Inside strawberry pyrite, around 20 μm in diameter, angular intercrystalline pores are often detected (Figure 5(f)). Longmaxi Formation shale mainly features organic bubble pores, followed by brittle mineral intragranular and intergranular pores. On the contrary, clay mineral pores are not well developed.

4.3. Analysis of Low-Temperature Nitrogen Adsorption. The marine shale and the marine-continental transitional shale display similar nitrogen adsorption isothermal patterns. The curve is an anti-S type as a whole, belonging to the typical type IV isotherm, and the hysteresis loop is equivalent to type H3 [21, 43] (Figure 6). At the beginning of adsorption, micropore filling and single-layer adsorption are completed quickly [55], and the adsorption quantity increases steeply. When the relative pressure increases to 0.8, the adsorption curve is relatively mild, suggesting the entry into a multilayer adsorption stage, and the adsorption quantity increases slowly by almost one time. When the relative pressure further increases to 1, capillary condensation takes place, the adsorption quantity quickly rises and is unsaturated. The maximum adsorption quantity of the marine shale is greater than that of the marine-continental transitional shale.

On the desorption branch, when the relative pressure decreases from 1 to 0.8, the gas in the half-open mesopores or macropores is quickly desorbed along the original path, causing the adsorption quantity to drop steeply. Then, the adsorption quantity drops slowly until the relative pressure decreases to nearby 0.5, when sudden evaporation causes the adsorption quantity to drop steeply again. After that, the adsorption curve almost coincides with the desorption curve. A hysteresis loop on the isotherm suggests the existence of mesopores in the sample. Obvious capillary condensation on the adsorption branch occurs at a pressure nearby 0.8 with no adsorption saturation, indicating that there are parallel plate pores with four edges open. Yet sudden evaporation takes place on the desorption branch at the relative pressure of 0.5, implying that there are thin bottleneck pores or ink bottle pores [35].

4.4. Analysis of Fractal. According to the FHH mesoporous fractal model, a scatter plot with the logarithm of the N_2 adsorption amount under a relative pressure ($\ln V$) as the horizontal axis and the double logarithm of the reciprocal of the relative pressure ($\ln\ln(p/p_0)$) as the vertical axis is shown in Figure 7. Since capillary condensation begins to appear when the relative pressure is greater than 0.5 (corresponding to the hysteresis loop), the adsorption data were divided into a low-pressure section with the relative pressure smaller than 0.5 and a high-pressure section with the relative pressure of 0.5-1, corresponding to Equations (3) and (4),

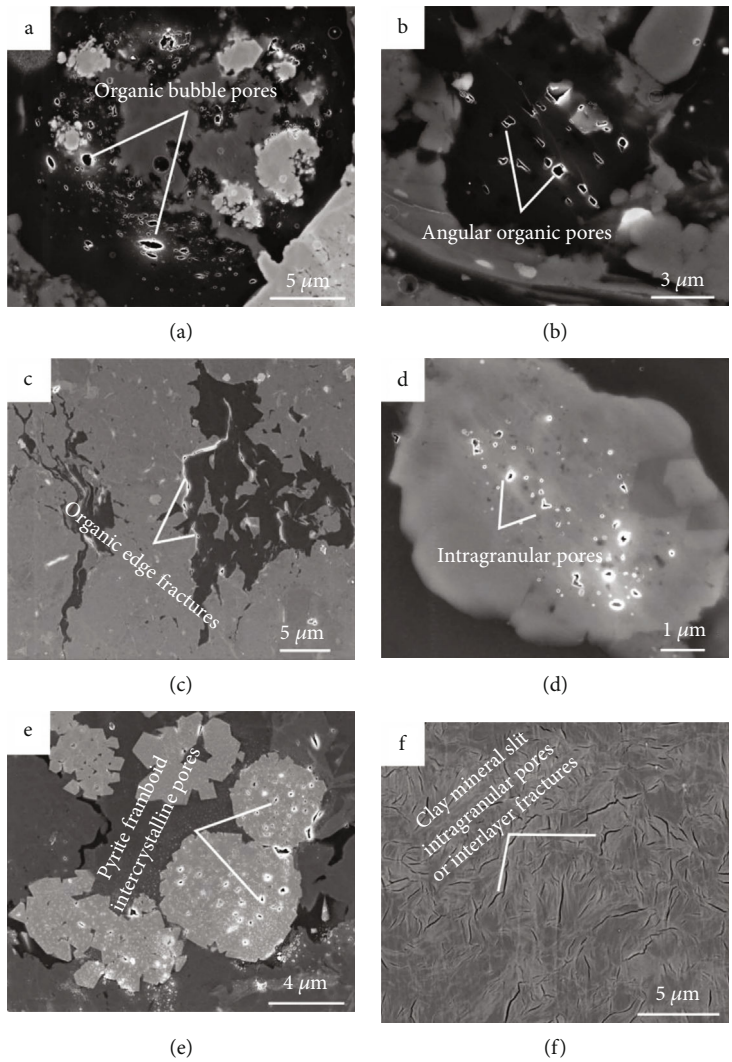

Figure 4: Different types of nanoscale pores in the marine-continental transitional shale. (a) Organic bubble pores. (b) Angular organic pores. (c) Organic edge fractures. (d) Intragranular pores. (e) Pyrite framboid intercrystalline pores. (f) Clay mineral slit intragranular pores or interlayer fractures.

respectively. For transitional shale, the fractal dimension in the low-pressure segment (D_1) is 1.7646–1.9944 with an average of 1.8670, and that in the high-pressure segment (D_2) is 2.5936–2.6716 with an average of 2.6368. For marine shale, D_1 is 2.0253–2.1666 with an average of 2.0779 and D_2 is 2.7260–2.7819 with an average of 2.7515 (Table 1).

5. Discussion

5.1. Pore Structure Characteristic Comparison. PSD curves derived from the BJH adsorption method can be used to determine the PSD of mesopores and some of the macropores. PSD curves can be plotted in two ways. Their ordinates are $dV/d(D)$ and $dV/d\log(D)$, respectively. Given that both shales contain few large pores and the second method can highlight the distribution of large pores, the second method was selected (Figure 8). The two shales differ obviously in PSD. In Shanxi Formation shale, the PSD curves vary considerably from one sample to another, but their general trend is quite the same, suggesting that transitional shale is highly heterogeneous. In Longmaxi Formation shale, the PSDs of mesopores are tight while those of macropores are loose, indicating that marine shale is less heterogeneous, but macropore development differs obviously among different layers. Comparison of the two shales shows that in terms of mesopores, marine shale is more developed than transitional shale, especially pores 2 nm–4 nm in size. For macropores, the two shales do not differ much, except that the change rate of pore volume in Shanxi Formation shale increases faster with the increase of pore size.

The BET specific surface area (SSA) and BJH total pore volume (PV) were compared to further investigate the pore structure differences between transitional shale and marine shale. For Shanxi Formation shale, the SSA is 2.1 m^2/g–12.4 m^2/g with an average of 9.1 m^2/g, the PV is 0.0049 ml/g–0.0314 ml/g with an average of 0.0245 ml/g, and the average pore diameter is 13.6 nm. In terms of Longmaxi Formation shale, the SSA is 19.3 m^2/g–28.2 m^2/g with

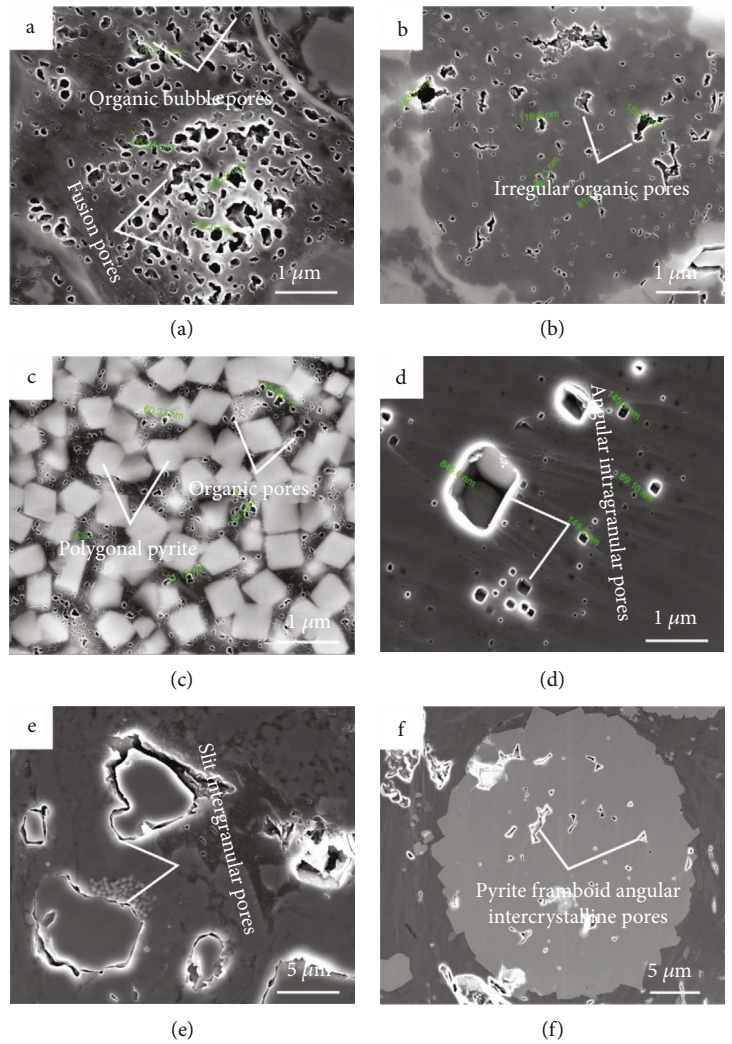

Figure 5: Different types of nanoscale pores in the marine shale. (a) Organic bubble pores. (b) Irregular organic pores. (c) Organic pores filled in pyrite particles. (d) Angular intragranular pores. (e) Slit intergranular pores. (f) Pyrite framboid angular intercrystalline pores.

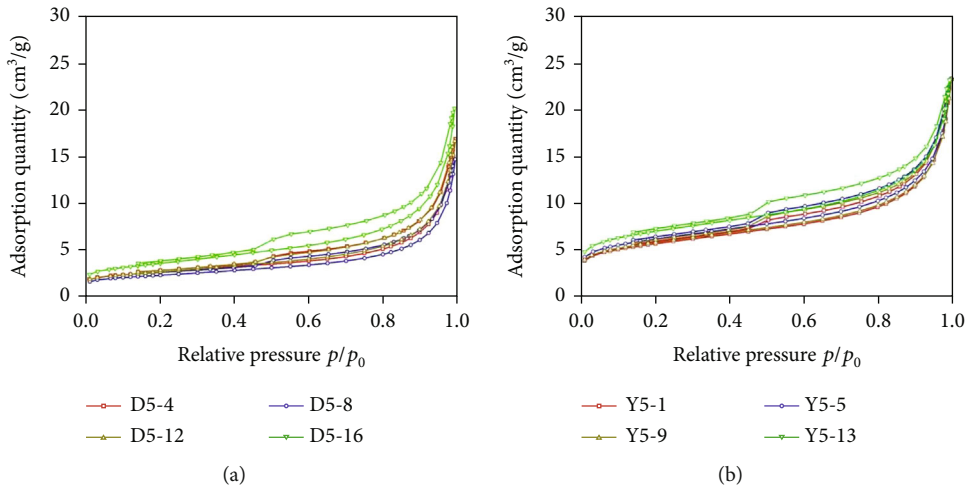

Figure 6: Typical sample N_2 isothermal adsorption graph of (a) Shanxi Formation shale and (b) Longmaxi Formation shale.

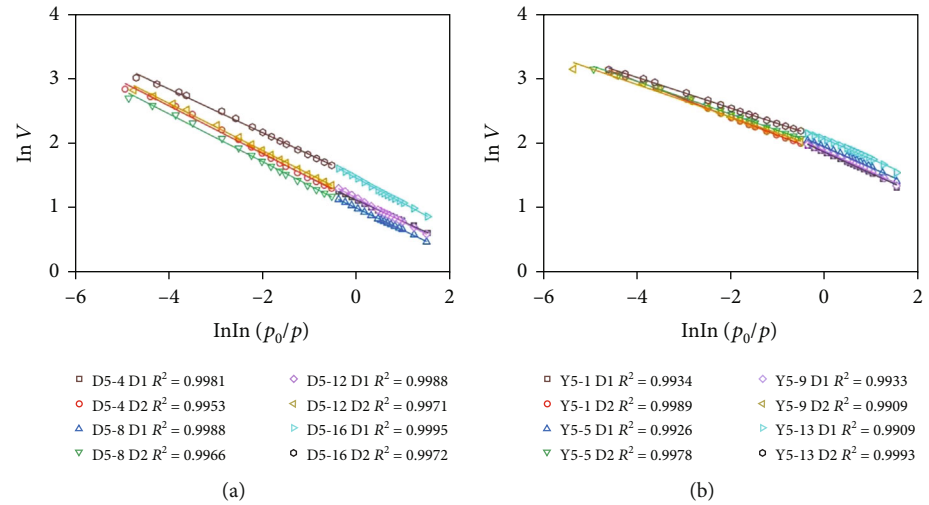

Figure 7: Typical sample mesopore fractal of (a) Shanxi Formation shale and (b) Longmaxi Formation shale.

Table 1: Mesopore fractal dimension comparison.

Sample ID	Relative pressure (0–0.5)		Relative pressure (0.5–1)		Sample ID	Relative pressure (0–0.5)		Relative pressure (0.5–1)	
	$f(D)$	D_1	$f(D)$	D_2		$f(D)$	D_1	$f(D)$	D_2
D5-4	0.3352	1.9944	0.3712	2.6288	Y5-1	0.2778	2.1666	0.2769	2.7231
D5-5	0.3521	1.9437	0.3862	2.6138	Y5-3	0.3249	2.0253	0.274	2.726
D5-6	0.3456	1.9632	0.3285	2.6715	Y5-5	0.3195	2.0415	0.2515	2.7485
D5-7	0.3809	1.8573	0.4064	2.5936	Y5-7	0.3213	2.0361	0.2695	2.7305
D5-10	0.3970	1.8090	0.3613	2.6387	Y5-9	0.3264	2.0208	0.2499	2.7501
D5-12	0.3771	1.8687	0.3663	2.6337	Y5-11	0.3187	2.0439	0.2499	2.7501
D5-14	0.3825	1.8525	0.3719	2.6281	Y5-13	0.3082	2.0754	0.2369	2.7631
D5-16	0.3907	1.8279	0.3393	2.6607	Y5-14	0.2963	2.1111	0.2308	2.7692
D5-18	0.4118	1.7646	0.3575	2.6425	Y5-15	0.2935	2.1195	0.2273	2.7727
D5-20	0.4039	1.7883	0.3439	2.6561	Y5-16	0.2870	2.1390	0.2181	2.7819

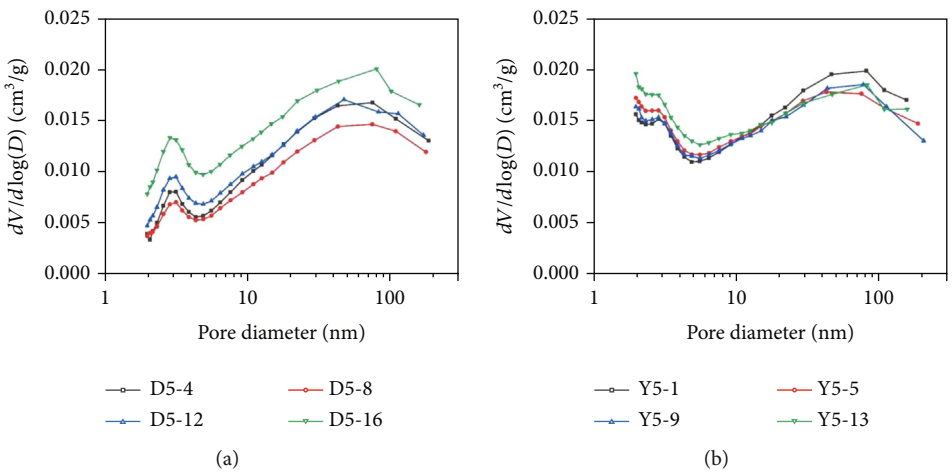

Figure 8: Typical sample PSD graph of (a) Shanxi Formation shale and (b) Longmaxi Formation shale.

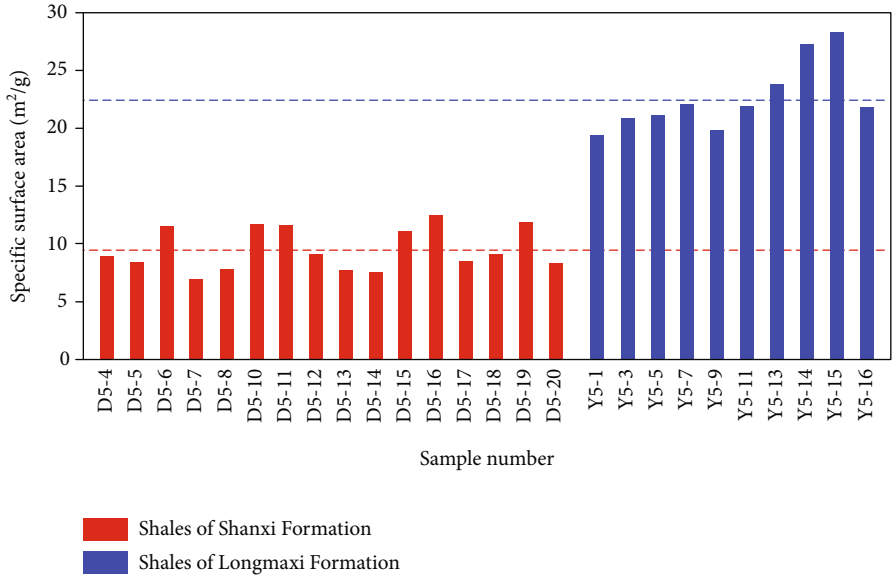

Figure 9: Comparative analysis results of the specific surface area between the two types of shale.

an average of 22.6 m^2/g, the PV is 0.0269 ml/g–0.0349 ml/g with an average of 0.0325 ml/g, and the average diameter is 9.5 nm. The results indicate that the two shales differ considerably in the pore structure. The SSA provided by most of the transitional shale samples is smaller than 10 m^2/g, which is about 1/2 of that of marine shale samples (Figure 9). The PV of Shanxi Formation shale is mostly in the 0.020 ml/g–0.030 ml/g range, while that of Longmaxi Formation shale is mostly larger than 0.030 ml/g (Figure 10). It suggests that smaller-sized pores are more developed in marine shale than in transitional shale, whereas the distribution of larger-sized pores does not differ much, which is consistent with our comparison of PSD.

5.2. Fractal Characteristic Comparison. The values of D_1 and D_2 represent the complexity of the pore structure corresponding to the low-pressure section and high-pressure section, respectively. Comparing the two fractal parameters of marine shale and marine-continental transitional shale, it is obvious that the D_1 and D_2 values of marine-continental transitional shale are smaller than those of marine shale (Figures 11 and 12), indicating that the complexity of the pore structure of marine-continental transitional shale is lower than that of marine shale. Because the transitional shale is dominated by mineral matrix pores, the marine shale is mainly composed of organic pores. Generally, the pore walls of organic pores are rougher than those of mineral matrix pores [56]. The fluctuation range of D_1 and D_2 of Shanxi Formation shale is larger than that of Longmaxi Formation shale, which indicates that the heterogeneity of Shanxi Formation shale is strong.

Further analysis of the relationship between the pore structure and the fractal dimension of marine-continental transitional shale and marine shale shows that the D_1 value has no obvious relationship with the specific surface area, but the D_2 value has a good positive correlation with the specific surface area (Figure 13). This is because the nitrogen adsorption in the low-pressure section involves a short micropore filling process, and the corresponding mesopore range in the low-pressure section is very small, which affects the result of the D_1 value. The more complex the mesopore structure corresponding to the high-pressure section, the larger the specific surface area and D_2 value will be.

5.3. Pore-Forming Mechanism Comparison and Its Geological Significance. Marine shale features well-developed organic pores and less-developed inorganic pores. Its geochemical data can verify that this shale has very good hydrocarbon-generating potential. The generation of gaseous hydrocarbon accompanies the entire process of organic matter evolution, including biogenic gas in the premature stage, pyrolysis gas (wet gas) in the mature stage, and cracked gas in the overmature stage (dry gas) [28–32]. The vitrinite reflectance of organic matter is mostly higher than 2.5% in Longmaxi Formation shale, indicating an overmature stage. In this stage, the liquid hydrocarbon and heavy gaseous hydrocarbon are cracked strongly to produce methane and bitumen. When the bitumen is not solidified, the pressure of the natural gas itself supports the bubble pores. Because the thickness of the marine shale is large, the natural gas is not easy to migrate out of the shale, and the bubble pores are the most affected by the deformation (Figure 14(b)). After the bitumen solidifies, these bubble pores are supported and protected by the solid bitumen skeleton and become the storage space of gaseous hydrocarbon [57].

The pore types of marine-continental transitional shale are different from those of marine shale, dominated by clay mineral slit pores and interlayer fractures and less developed organic matter pores. Organic geochemical analysis shows that the marine-continental transitional shale is also in the over mature stage, but the type III organic matter means that the marine-continental transitional shale directly generates gaseous hydrocarbon in the form of kerogen degradation, and only a small amount of liquid hydrocarbon is generated,

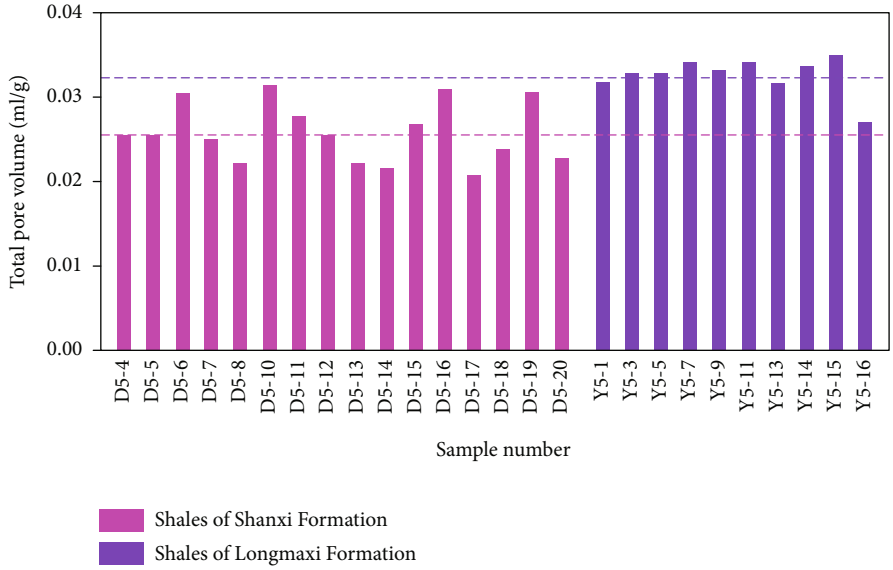

Figure 10: Comparative analysis results of the total pore volume between the two types of shale.

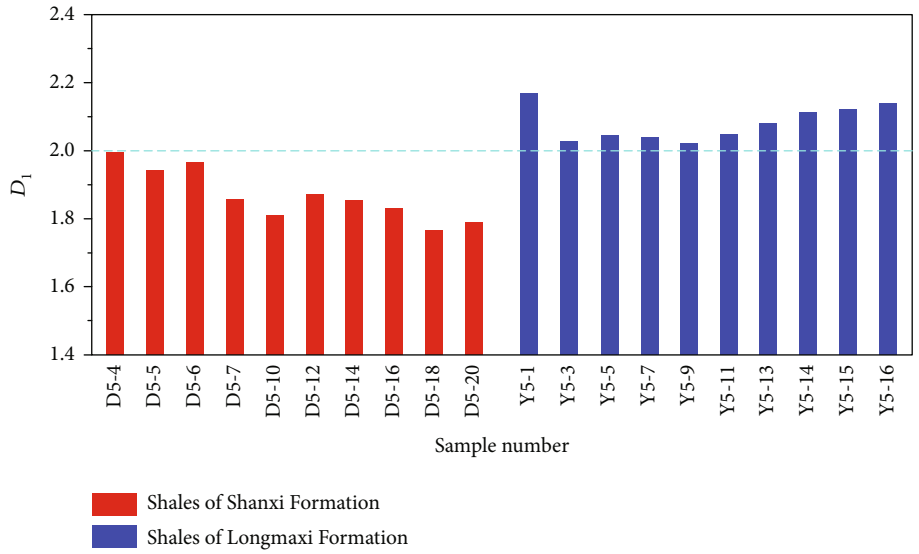

Figure 11: Comparative analysis results of the D_1 value between the two types of shale.

then cracking to generate gaseous hydrocarbon. Therefore, there are only a few organic matter bubble pores in the transitional shale [58, 59]. It can be seen that the type of organic matter is one of the influencing factors of pore development.

The on-site gas content test shows that the field gas content of shale samples in well D5 is 0.21 m^3/t–3.71 m^3/t with an average of 1.39 m^3/t, and that in well Y5 is 1.88 m^3/t–6.18 m^3/t with an average of 2.92 m^3/t. The gas hydrocarbon content of transitional shale is lower than that of marine shale, but in the sandstone layer adjacent to the Shanxi Formation shale layer, the gas content is comparable to that of the shale layer, suggesting that part of the gaseous hydrocarbon produced from the shale layer has been migrated to the sandstone layer. This is because the depositional environment of Shanxi Formation shale in the eastern Ordos Basin is deltaic facies featuring frequent sand-mud alternation and high hydrocarbon expulsion efficiency in the stratum. Large amounts of the natural gas produced from the shale can easily be migrated into the adjacent tight sandstone to form conventional gas reservoirs (Figure 14(a)). A large number of connected clay mineral slit-like pores and interlayer fractures provide migration channels so that natural gas can migrate to adjacent sandstone, resulting in the organic matter pores not being preserved. At the same time, the mineral matrix pores of shale also provide space for shale gas preservation. Therefore, the sedimentary environment is also an important factor affecting the pore development of marine-continental transitional shale [34, 60].

Although a large amount of natural gas in the shale layer migrated to the adjacent sandstone layer, the average gas content of the shale reservoir is still 1.39 m^3/t, which not only indicates that there are a large number of mineral matrix

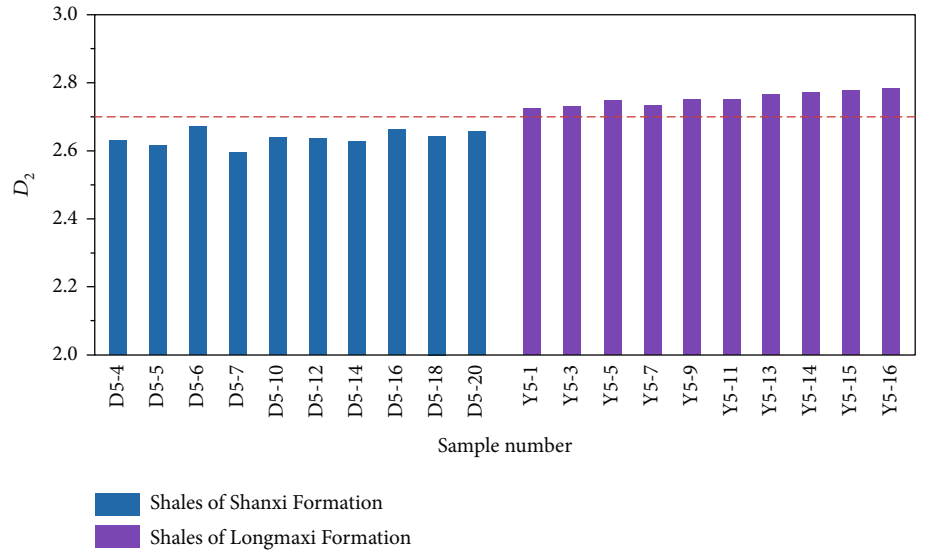

Figure 12: Comparative analysis results of the D_2 value between the two types of shale.

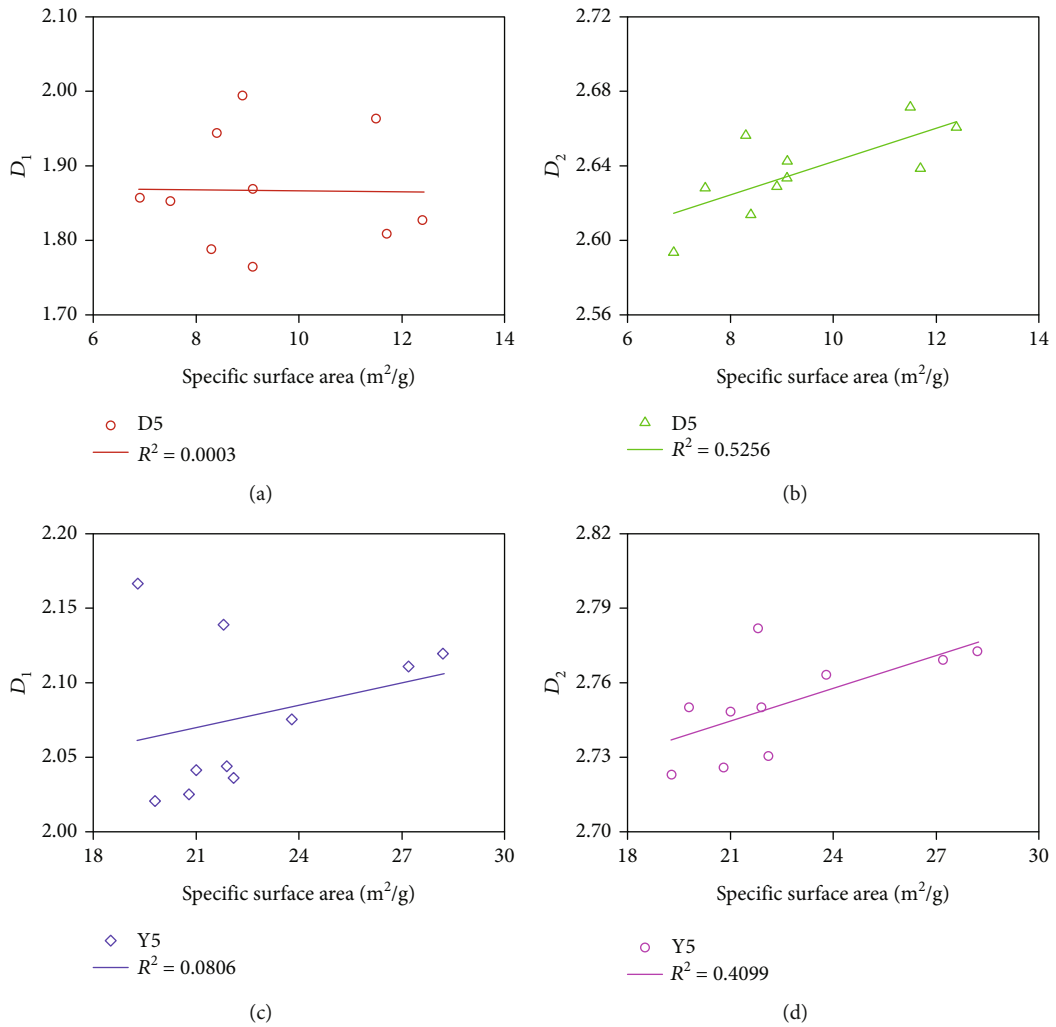

Figure 13: Relationship between the fractal dimension and the specific surface area of (a, b) Shanxi Formation shale and (c, d) Longmaxi Formation shale.

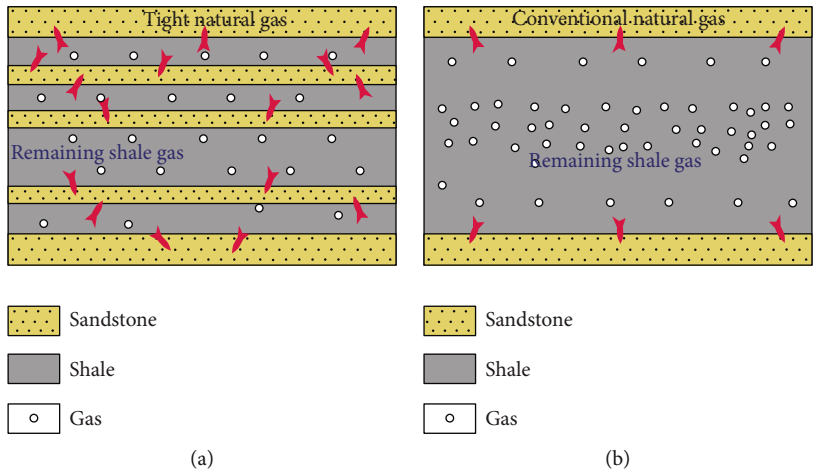

Figure 14: Hydrocarbon expulsion model of (a) Shanxi Formation shale and (b) Longmaxi Formation shale.

pores to provide storage space but also indicates that the adjacent single shale and single sandstone provide better sealing conditions for each other when the hydrocarbon concentration reaches a certain value so as to prevent the further transportation of natural gas. Therefore, the exploration target of the Shanxi Formation in the eastern Ordos Basin should not be limited to shale strata only. It is suggested that the combination of interbedded mudrock and sandstone can be taken as the key exploration target for the Shanxi Formation marine-continental transitional stratum in the eastern Ordos Basin.

6. Conclusions

(1) The clay minerals of the Shanxi Formation are more developed than quartz minerals, dominated by clay mineral slit pores and interlayer fractures, followed by brittle mineral intragranular pores. The quartz contents of Longmaxi Formation shale are higher than clay contents, mainly composed of organic matter nanopores, and mineral matrix pores are less developed

(2) The shapes of the nitrogen adsorption curves of the marine and transitional shales are similar, showing parallel plate pores and ink bottle pores. Longmaxi Formation shale with more mesopores has a larger SSA and a more complex pore structure

(3) The type of organic matter (type I or III) and the sedimentary environment are important influencing factors of the development of organic nanopores. Mineral matrix pores with good connectivity can also affect the formation of organic pores to a certain degree

(4) The transitional shale features frequent sand-mud alternation and cannot completely preserve gaseous hydrocarbon. Its exploration target can be focused on the combination of interbedded mudrock and sandstone

Data Availability

The data used to support the findings of this study are included within the article.

Conflicts of Interest

The authors declare that they have no conflicts of interest.

Acknowledgments

This study was funded by the National Science and Technology Major Project (No. 2017ZX05035002-002).

References

[1] C. Zou, Q. Zhao, D. Dong et al., "Geological characteristics, main challenges and future prospect of shale gas," *Journal of Natural Gas Geoscience*, vol. 2, no. 5-6, pp. 273–288, 2017.

[2] X. Guo, Y. Li, B. Tenger et al., "Hydrocarbon generation and storage mechanisms of deep-water shelf shales of Ordovician Wufeng Formation-Silurian Longmaxi Formation in Sichuan Basin," *Petroleum Exploration and Development*, vol. 47, no. 1, pp. 193–201, 2020.

[3] Z. Jiang, Y. Song, X. Tang et al., "Controlling factors of marine shale gas differential enrichment in southern China," *Petroleum Exploration and Development*, vol. 47, no. 3, pp. 417–628, 2020.

[4] C. Zou, D. Dong, Y. Wang et al., "Shale gas in China: characteristics, challenges and prospects (I)," *Petroleum Exploration and Development*, vol. 42, no. 6, pp. 689–701, 2015.

[5] X. Ma, H. Wang, S. Zhou, Z. Feng, H. Liu, and W. Guo, "Insights into NMR response characteristics of shales and its application in shale gas reservoir evaluation," *Journal of Natural Gas Science and Engineering*, vol. 84, article 103674, 2020.

[6] Y. Ma, M. Fan, Y. Lu et al., "Geochemistry and sedimentology of the Lower Silurian Longmaxi mudstone in southwestern China: implications for depositional controls on organic matter accumulation," *Marine and Petroleum Geology*, vol. 75, pp. 291–309, 2016.

[7] X. Guo, "Controlling factors on shale gas accumulations of Wufeng-Longmaxi Formations in Pingqiao shale gas field in Fuling area, Sichuan Basin," *Natural Gas Geoscience*, vol. 30, no. 1, pp. 1–10, 2019.

[8] S. Liu, W. Ma, L. Jansa, W. Huang, X. Zeng, and C. Zhang, "Characteristics of the shale gas reservoir rocks in the Lower Silurian Longmaxi Formation, East Sichuan Basin, China," *Acta Petrologica Sinica*, vol. 27, no. 8, pp. 2239–2252, 2011.

[9] C. Liang, Z. Jiang, C. Zhang, L. Guo, Y. Yang, and J. Li, "The shale characteristics and shale gas exploration prospects of the Lower Silurian Longmaxi Shale, Sichuan Basin, South China," *Journal of Natural Gas Science and Engineering*, vol. 21, pp. 636–648, 2014.

[10] M. Sun, B. Yu, Q. Hu, S. Chen, W. Xia, and R. Ye, "Nanoscale pore characteristics of the Lower Cambrian Niutitang Formation Shale: a case study from Well Yuke 1 in the Southeast of Chongqing, China," *International Journal of Coal Geology*, vol. 154-155, pp. 16–29, 2016.

[11] T. Cao, Z. Song, S. Wang, X. Cao, Y. Li, and J. Xia, "Characterizing the pore structure in the Silurian and Permian shales of the Sichuan Basin, China," *Marine and Petroleum Geology*, vol. 61, pp. 140–150, 2015.

[12] J. Shu, Y. Peng, B. Gao et al., "Geology and shale gas resource potentials in the Sichuan Basin, China," *Energy Exploration and Exploitation*, vol. 34, no. 5, pp. 689–710, 2016.

[13] S. Chen, Y. Zhu, H. Wang, H. Liu, W. Wei, and J. Fang, "Characteristics and significance of mineral compositions of Lower Silurian Longmaxi Formation Shale gas reservoir in the southern margin of Sichuan Basin," *Acta Petrolei Sinica*, vol. 32, no. 5, pp. 775–782, 2011.

[14] X. Wang, C. Mou, X. Ge et al., "Mineral component characteristics and evaluation of black rock series of Longmaxi Formation in Southern Sichuan and its periphery," *Acta Petrolei Sinica*, vol. 36, no. 2, pp. 150–162, 2015.

[15] H. Zhang, X. Jin, J. Wu, Q. Yang, and L. Hao, "Nano-pores of organic matter in Longmaxi Formation shale in Sichuan Basin," *Coal Geology & Exploration*, vol. 46, no. 3, pp. 47–53, 2018.

[16] H. Nie, Z. Jin, C. Sun, Z. He, G. Liu, and Q. Liu, "Organic matter types of the Wufeng and Longmaxi Formations in the Sichuan Basin, South China: implications for the formation of organic matter pores," *Energy Fuels*, vol. 33, no. 9, pp. 8076–8100, 2019.

[17] R. G. Loucks and R. M. Reed, "Scanning-electron-microscope petrographic evidence for distinguishing organic-matter pores associated with depositional organic matter versus migrated organic matter in mudrocks," *Gulf Coast Association of Geological Societies*, vol. 3, pp. 51–60, 2014.

[18] J. Rouquerol, D. Avnir, C. W. Fairbridge et al., "Recommendations for the characterization of porous solids (technical report)," *Pure & Applied Chemistry*, vol. 66, no. 8, pp. 1739–1758, 1994.

[19] H. Hu, F. Hao, J. Lin, Y. Lu, Y. Ma, and Q. Li, "Organic matter-hosted pore system in the Wufeng-Longmaxi (O_3w-S_1l) shale, Jiaoshiba area, Eastern Sichuan Basin, China," *International Journal of Coal Geology*, vol. 173, pp. 40–50, 2017.

[20] K. Jiao, S. Yao, C. Liu et al., "The characterization and quantitative analysis of nanopores in unconventional gas reservoirs utilizing FESEM-FIB and image processing: an example from the Lower Silurian Longmaxi Shale, upper Yangtze region, China," *International Journal of Coal Geology*, vol. 128-129, pp. 1–11, 2014.

[21] K. Liu, M. Ostadhassan, and L. Kong, "Multifractal characteristics of Longmaxi Shale pore structures by N2 adsorption: a model comparison," *Journal of Petroleum Science and Engineering*, vol. 168, pp. 330–341, 2018.

[22] F. Wang, J. Guan, W. Feng, and L. Bao, "Evolution of overmature marine shale porosity and implication to the free gas volume," *Petroleum Exploration and Development*, vol. 40, no. 6, pp. 819–824, 2013.

[23] L. Wu, Y. Lu, S. Jiang, Y. Lu, X. Liu, and H. Hu, "Pore structure characterization of different lithofacies in marine shale: a case study of the Upper Ordovician Wufeng-Lower Silurian Longmaxi Formation in the Sichuan Basin, SW China," *Journal of Natural Gas Science and Engineering*, vol. 57, pp. 203–215, 2018.

[24] T. Cao, M. Deng, Z. Song, G. Liu, Y. Huang, and A. S. Hursthouse, "Study on the effect of pyrite on the accumulation of shale oil and gas," *Natural Gas Geoscience*, vol. 29, no. 3, pp. 404–414, 2018.

[25] X. Tang, Z. Jiang, Z. Li et al., "The effect of the variation in material composition on the heterogeneous pore structure of high-maturity shale of the Silurian Longmaxi Formation in the southeastern Sichuan Basin, China," *Journal of Natural Gas Science and Engineering*, vol. 23, pp. 464–473, 2015.

[26] S. Chen, Y. Han, C. Fu, H. Zhang, Y. Zhu, and Z. Zuo, "Micro and nano-size pores of clay minerals in shale reservoirs: implication for the accumulation of shale gas," *Sedimentary Geology*, vol. 342, pp. 180–190, 2016.

[27] Y. Wang, D. Dong, H. Yang et al., "Quantitative characterization of reservoir space in the Lower Silurian Longmaxi Shale, Southern Sichuan, China," *Science China: Earth Sciences*, vol. 57, no. 2, pp. 313–322, 2014.

[28] L. T. Ko, R. G. Loucks, T. Zhang, S. C. Ruppel, and D. Shao, "Pore and pore network evolution of upper Cretaceous Boquillas (Eagle Ford-equivalent) mudrocks: results from gold tube pyrolysis experiments," *AAPG Bulletin*, vol. 100, no. 11, pp. 1693–1722, 2016.

[29] L. T. Ko, R. G. Loucks, S. C. Ruppel, T. Zhang, and S. Peng, "Origin and characterization of Eagle Ford pore networks in the South Texas upper Cretaceous shelf," *AAPG Bulletin*, vol. 101, no. 3, pp. 387–418, 2017.

[30] S. Bernard, R. Wirth, A. Schreiber, H. M. Schulz, and B. Horsfield, "Formation of nanoporous pyrobitumen residues during maturation of the Barnett Shale (Fort Worth Basin)," *International Journal of Coal Geology*, vol. 103, pp. 3–11, 2012.

[31] H. Liu, X. Li, and S. Zhou, "Phenomenon of bubble evolving into pore occurred in black shale and its geological significance," *Natural Gas and Oil*, vol. 36, no. 6, pp. 60–64, 2018.

[32] S. C. Löhr, E. T. Baruch, P. A. Hall, and M. J. Kennedy, "Is organic pore development in gas shales influenced by the primary porosity and structure of thermally immature organic matter?," *Organic Geochemistry*, vol. 87, pp. 119–132, 2015.

[33] C. Yang, J. Zhang, S. Han et al., "Compositional controls on pore-size distribution by nitrogen adsorption technique in the Lower Permian Shanxi Shales, Ordos Basin," *Journal of Natural Gas Science and Engineering*, vol. 34, pp. 1369–1381, 2016.

[34] J. Liu, K. Liu, and X. Huang, "Effect of sedimentary heterogeneities on hydrocarbon accumulations in the Permian Shanxi Formation, Ordos Basin, China: insight from an integrated

stratigraphic forward and petroleum system modelling," *Marine and Petroleum Geology*, vol. 76, pp. 412–431, 2016.

[35] L. Kuang, D. Dong, W. He et al., "Geological characteristics and development potential of transitional shale gas in the east margin of the Ordos Basin, NW China," *Petroleum Exploration and Development*, vol. 47, no. 3, pp. 435–446, 2020.

[36] Z. Wei, G. Wang, Y. Wang et al., "Geochemical and geological characterization of marine-continental transitional shale: a case study in the Ordos Basin, NW China," *Acta Geologica Sinica*, vol. 94, no. 3, pp. 809–821, 2020.

[37] C. Xue, J. Wu, L. Qiu et al., "Lithofacies classification and its controls on the pore structure distribution in Permian transitional shale in the northeastern Ordos Basin, China," *Journal of Petroleum Science and Engineering*, vol. 195, article 107657, 2020.

[38] X. Tang, H. Zhang, W. Ding et al., "The reservoir property of the Upper Paleozoic marine-continental transitional shale and its gas-bearing capacity in the Southeastern Ordos Basin," *Earth Science Frontiers*, vol. 23, no. 2, pp. 147–157, 2016.

[39] P. Zhang, Y. Huang, J. Zhang, H. Liu, and J. Yang, "Fractal characteristics of the Longtan Formation transitional shale in northwest Guizhou," *Journal of China Coal Society*, vol. 43, no. 6, pp. 1580–1588, 2018.

[40] D. Zhao, Y. Guo, C. Ren, and Y. Li, "Development characteristics and affecting factors of nanopores in transitional shale reservoirs: an example of the Shanxi Formation," *Journal of Northeast Petroleum University*, vol. 42, no. 5, pp. 1–15, 2018.

[41] J. Zhang, X. Li, Y. Wang, Q. Fu, Y. Cai, and H. Niu, "Accumulation conditions and reservoir characteristics of marine-terrigenous facies coal measures shale gas from Longtan Formation in South Sichuan Basin," *Journal of China Coal Society*, vol. 40, no. 8, pp. 1871–1878, 2015.

[42] S. Tang, J. Zhang, D. Elsworth et al., "Lithofacies and pore characterization of the Lower Permian Shanxi and Taiyuan shales in the southern North China Basin," *Journal of Natural Gas Science and Engineering*, vol. 36, pp. 644–661, 2016.

[43] F. Xiong, Z. Jiang, P. Li et al., "Pore structure of transitional shales in the Ordos Basin, NW China: effects of composition on gas storage capacity," *Fuel*, vol. 206, pp. 504–515, 2017.

[44] T. Cao, Q. Cao, H. Liu, M. Deng, and G. Liu, "Geochemical characteristics and adsorption capacity of marine-continental transitional mudrock in eastern Sichuan Basin," *Journal of China Coal Society*, vol. 45, no. 4, pp. 241–252, 2020.

[45] E. Deng, J. Jin, R. Wang, F. Shi, and L. Wang, "Characteristics of microscopic pore and gas storage on shale in Permian Longtan Formation, Northern Guizhou," *Science Technology and Engineering*, vol. 17, no. 24, pp. 190–195, 2017.

[46] Z. Xi, S. Tang, J. Li, and L. Li, "Investigation of pore structure and fractal characteristics of marine-continental transitional shale in the east-central of Qinshui Basin," *Natural Gas Geoscience*, vol. 28, no. 3, pp. 366–376, 2017.

[47] Z. P. Sun, Y. L. Wang, Z. F. Wei et al., "Shale gas content and geochemical characteristics of marine-continental transitional shale: a case from the Shanxi Formation of Ordos Basin," *Journal of China University of Mining & Technology*, vol. 46, no. 4, pp. 859–868, 2017.

[48] Q. Gou, S. Xu, F. Hao, F. Yang, Z. Shu, and R. Liu, "The effect of tectonic deformation and preservation condition on the shale pore structure using adsorption-based textural quantification and 3D image observation," *Energy*, vol. 219, p. 119579, 2021.

[49] S. Zhou, G. Yan, H. Xue, W. Guo, and X. Li, "2D and 3D nanopore characterization of gas shale in Longmaxi Formation based on FIB-SEM," *Marine and Petroleum Geology*, vol. 73, pp. 174–180, 2016.

[50] S. Brunauer, P. H. Emmett, and E. Teller, "Adsorption of gases in multimolecular layers," *Journal of the American Chemical Society*, vol. 60, no. 2, pp. 309–319, 1938.

[51] E. P. Barrett, L. G. Joyner, and P. H. Halenda, "The determination of pore volume and area distributions in porous substances. I. Computations from nitrogen isotherms," *Journal of the American Chemical Society*, vol. 73, no. 1, pp. 193–380, 1951.

[52] S. Zhou, D. Zhang, H. Wang, and X. Li, "A modified BET equation to investigate supercritical methane adsorption mechanisms in shale," *Marine and Petroleum Geology*, vol. 105, pp. 284–292, 2019.

[53] J. Liu, D. Lu, and P. Li, "Nano-scale dual-pore-shape structure and fractal characteristics of transitional facies shale matrix," *Journal of Natural Gas Science and Engineering*, vol. 68, article 102907, 2019.

[54] M. K. Ismail and P. Pfeifer, "Fractal analysis and surface roughness of nonporous carbon fibers and carbon blacks," *Langmuir*, vol. 10, no. 5, pp. 1532–1538, 1994.

[55] S. Zhou, Y. Ning, H. Wang, H. Liu, and H. Xue, "Investigation of methane adsorption mechanism on Longmaxi shale by combining the micropore filling and monolayer coverage theories," *Advances in Geo-Energy Research*, vol. 2, no. 3, pp. 269–281, 2018.

[56] X. Shao, X. Pang, Q. Li et al., "Pore structure and fractal characteristics of organic-rich shales: a case study of the Lower Silurian Longmaxi shales in the Sichuan Basin, SW China," *Marine and Petroleum Geology*, vol. 80, pp. 192–202, 2017.

[57] X. Li, G. Chen, Z. Chen et al., "An insight into the mechanism and evolution of shale reservoir characteristics with over-high maturity," *Natural Gas Geoscience*, vol. 27, no. 3, pp. 407–416, 2016.

[58] T. Zhang, G. S. Ellis, S. C. Ruppel, K. Milliken, and R. Yang, "Effect of organic-matter type and thermal maturity on methane adsorption in shale-gas systems," *Organic Geochemistry*, vol. 47, pp. 120–131, 2012.

[59] J. Zhao, J. Zhang, and G. Gao, *Geology of Natural Gas*, Petroleum Industry Press, Beijing, 2013.

[60] H. Liu, H. Wang, H. Zhang, W. Zhao, Y. Liu, and D. Liu, "Geological characteristics and exploration countermeasures of shale gas in the Shanxi Formation of the Ordos Basin," *Acta Geologica Sinica*, vol. 94, no. 3, pp. 905–915, 2020.